ACS OMEGA

Open Access

http://pubs.acs.org/journal/acsodf

Article

Biosolid Gasification Performance Prediction Using a Stoichiometric Thermodynamic Model

Fangtian Li, Xin Zhang, and Yun Ji*

Cite This: *ACS Omega* 2024, 9, 32639−32650

Read Online

ACCESS | Metrics & More | Article Recommendations | Supporting Information

ABSTRACT: The gasification process can recover energy from biosolids produced in wastewater treatment. This paper developed a stoichiometric thermodynamic equilibrium model for biosolid gasification based on the biosolid properties, thermodynamic database, and equilibrium constants. If the calculation result showed that the quantity of char was negative, the quantity of char was put to zero, and the simulation was carried out again. The model was first verified by woody gasification under isothermal conditions, and the influence of a given temperature on biosolid gasification was simulated. The model further investigated the effects of different feedstock types, moisture contents, equivalence ratios, and reaction extensions on the adiabatic temperature, exergy efficiency, and syngas properties under autothermal conditions. The four factors were all the main factors for adiabatic temperature. The exergy efficiency depended more on the operation conditions than on the feedstock type. The H_2 concentration of the dry syngas in biosolid gasification exhibited a curve both against the given temperature under isothermal conditions and against the moisture content under autothermal conditions.

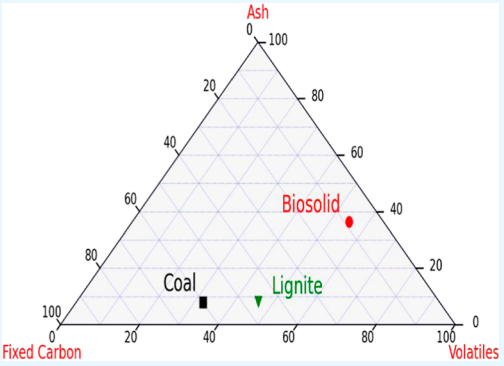

1. INTRODUCTION

The increasing demand for new alternative energy supply arises from the depletion and the environmental impact of conventional fossil fuel resources.[1] Various renewable energy sources, such as biomass, have received much attention worldwide. Meanwhile, increasing amounts of biosolids (treated sewage sludge) are being produced continuously as byproducts in municipal wastewater treatments.[2] The biosolids contain certain hydrocarbon materials and could be utilized as special biomass, based on carbon, hydrogen, and oxygen percentages.[3] The heating values in the biosolids can be recovered through the sludge-to-energy technologies.[4,5]

Popular biosolid disposal methods include landfilling, agriculture applications, biochemical treatments, and thermochemical processes.[6,7] However, the first two disposal methods of biosolids face unsustainability challenges due to land limitations and more stringent environmental regulations.[8] Both biochemical and thermochemical processes are waste-to-energy solutions. Biochemical methods, such as anaerobic digestion, are prevalent for biogas production, but they normally take a long residence time (20−30 days), large space, and low efficiency (30−50%) of organic matter decomposition.[9] In contrast, thermochemical processes convert biosolids into gaseous and liquid fuels and other chemical substances within a short period under high-temperature conditions. These processes include pyrolysis, gasification, and combustion, conducted under oxygen-free, oxygen-depleted, or oxygen-excess conditions, respectively.[10,11]

Pyrolysis and gasification, in contrast to combustion, decompose the biosolids thermally into their gaseous, liquid, and solid (biochar) fractions at intermediate and high temperatures, respectively.[12]

Biosolid gasification has become one of the most promising thermochemical conversion processes. Gasification can convert a wide variety of feedstocks such as coal, biomass, and residues into syngas after heat recovery and purification. The syngas mainly consists of H_2, CO, CO_2, CH_4, and other lightweight hydrocarbons,[13] and its composition depends on the variety of feedstock, reaction temperature, and pressure conditions as well as the gasifying agent: air, oxygen, steam, or carbon dioxide. Serving as an intermediate for subsequent uses, syngas can be directly used as a clean and efficient fuel for heat and electricity generation or further processed into high-value chemicals, such as hydrogen, substitute natural gas, Fischer−Tropsch (FT) fuel, and methanol.[14]

The biosolid gasification process can be simulated effectively by theoretical modeling to study the influence of various operational and design parameters on the producer gas quality and optimize the process. The main modeling approaches

Received: February 21, 2024
Revised: July 9, 2024
Accepted: July 10, 2024
Published: July 17, 2024

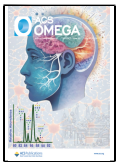

https://doi.org/10.1021/acsomega.4c01687
ACS Omega 2024, 9, 32639−32650

include thermodynamic equilibrium models, kinetics models, computational fluid dynamics (CFD), and the artificial neural network (ANN).[15,16] The thermodynamic equilibrium model predicts the biomass gasification production composition based on the reaction equilibrium assumption. It is a convincing approximation of the syngas composition and predicts the maximum achievable yields.[17] The kinetic model takes into account detailed reaction kinetics, system hydrodynamics, and particle size distribution and gives the syngas concentrations at any time within the system.[18] CFD is based on the finite difference or finite element methods coupled with reaction, mass, heat, and momentum conversion equations and is used to guide reactor design and troubleshooting, but lots of computing resources are needed at the same time.[19] The ANN belongs to black-box models and makes use of regression to correlate input and output streams based on a large number of reliable data points.[20]

Among the four model methods, thermodynamic equilibrium is simple and fast in calculation compared with other models and independent of reaction mechanisms and the gasifier structure.[21] The thermodynamic equilibrium approach predicts the composition of the outlet gases based on the assumption that the components react in a fully mixed condition for an infinite period; however, gasification is much more complicated, and an equilibrium state may not be achieved for all reactions in some parts of the gasifier due to the short residence time of gases in the reactor. Thermodynamic equilibrium models can be divided into stoichiometric and nonstoichiometric approaches,[17] based on reaction equilibrium constants and direct minimization of Gibbs free energy, respectively. The stoichiometric thermodynamic equilibrium model combines overall mass balance, energy balance, and thermodynamic equilibrium reaction equations to be solved.[22−24]

Exergy is a very useful method to evaluate the thermodynamic and energy performances of various chemical processes. Exergy stands for the potential of energy to work (maximum possible work obtained from the system) based on the reference environment.[25] Exergy efficiency is the ratio of the total exergy of the outlet stream of a system to the total exergy of the inlet stream of the system.[24] Exergy analysis can provide a better understanding of the amount of energy utilization and quantify the irreversibility of the system.[26,27] It is applicable to optimize the biosolid gasification process.

This paper develops a stoichiometric thermodynamic equilibrium model for biosolid gasification based on the biosolid properties, thermodynamic database, and equilibrium constants. The biosolid gasification process is simulated under isothermal conditions to verify the model and autothermal conditions to examine the effects of different feedstock types, moisture content, equivalence ratio (ER), and reaction extension on adiabatic temperature, exergy efficiency, moles of dry syngas, the concentration of H_2, CO, and CH_4, and cold-gas efficiency (CGE).

2. BIOSOLID PROPERTIES AND BASIC THERMOCHEMICAL DATA

2.1. Biosolid Properties. The typical biomass composition consists of organic, inorganic, and water components. In the gasification process, the organic part is converted to syngas and char by the gasification agents, the inorganic components are discharged in the form of ashes, and the liquid water is vaporized first.

The biosolid is commonly described by proximate and ultimate analysis. In proximate analysis, the moisture content is as received shown as M_{ar}, and the ash is based on a dry base shown as A_d. Their relationship is illustrated in Table 1.

Table 1. Relationship of Proximate Analysis Elements of the Biosolid

base	organic part	ash dry	moisture
As received	$1 - M_{ar}$		M_{ar}
dry base	$1 - A_d$	A_d	0

As the moisture varies among the different materials, a dry base is always used to compare their organic components. The volatile part and fixed carbon combine with the organic part of the biosolid. The proximate analysis comparison of different feedstocks is illustrated in Table 2 and Figure 1. The biosolid has more ashes than other common fuels on a dry base.

Table 2. Proximate Analysis of Different Feedstocks, wt %[a]

	volatile	fixed carbon	ash	moisture	sum	base
Shenhua coal[28]	29.6	55.0	7.21	8.28	100	ar.
	32.2	**59.9**	**7.9**	**0**	**100**	**db.**
lignite coal near the center, ND[29]	29.0	28.9	5.1	37.1	100	ar.
	46.0	**45.9**	**8.1**	**0**	**100**	**db.**
biosolid[30]	17.1	2.73	11.3	68.8	100	ar.
	54.9	**8.8**	**36.3**	**0**	**100**	**db.**

[a]Where ar. means as received and db. means dry base.

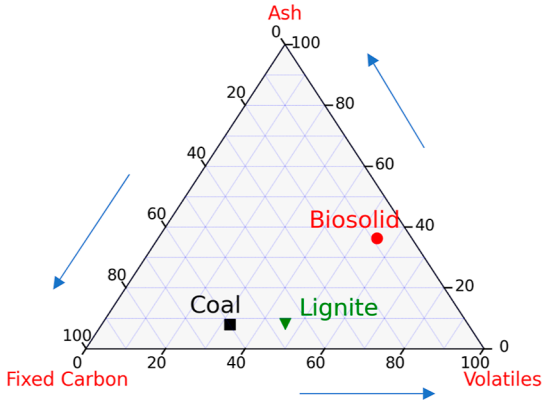

Figure 1. Ternary diagram of proximate analysis, wt % (dry base).

The ultimate analysis shows the mass fraction of carbon, hydrogen, oxygen, nitrogen, and sulfur in the organic part of the biosolid. The ultimate analysis comparison of different feedstocks is illustrated in Table 3 and Figure 2.

From the mass composition of the biomass, the chemical formula of biomass composition can be obtained. The organic part is depicted in $CH_wO_xN_yS_z$, based on a single atom of carbon, and the value of w, x, y, and z can be calculated from ultimate analysis as shown in Table 4. Therefore, the biosolid can be represented as $CH_wO_xN_yS_z$ + ash + H_2O, and the dry biosolid is $CH_wO_xN_yS_z$ + ash.

The heating value of the biosolid depends on the biosolid composition. The form enthalpy is calculated through the higher heating value (HHV), which could be estimated by ultimate analysis as eq 1.[32]

https://doi.org/10.1021/acsomega.4c01687
ACS Omega 2024, 9, 32639−32650

Table 3. Ultimate Analysis of Different Feedstocks, wt %[a]

	C	H	O*	N	S	sum	base
Shenhua coal[28]	69.6	3.74	10.1	0.83	0.25	84.5	ar.
	82.3	**4.4**	**12.0**	**1.0**	**0.3**	**100**	**daf.**
lignite coal near the center, ND[29]	40.9	7.0	45.8	0.5	0.7	94.2	ar.
	43.1	**7.4**	**48.3**	**0.5**	**0.7**	**100**	**daf.**
biosolid[30]	9.94	1.43	6.17	1.5	0.82	19.9	ar.
	50.1	**7.2**	**31.1**	**7.6**	**4.1**	**100**	**daf.**
woody biomass[31]	**50**	**6**	**44**	**0**	**0**	**100**	**daf**

[a]Where O* is derived by difference, ar. means as received, and daf. means dry ash-free.

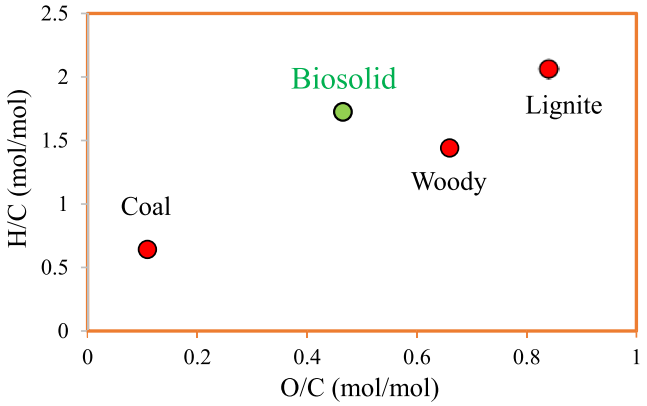

Figure 2. Van Krevelen diagram for samples based on ultimate analysis (dry ash-free).

Table 4. Molecular Relationship of the Feedstocks

	C	H	O	N	S
feedstock		*w*	*x*	*y*	*z*
woody	1	1.43	0.66	0	0
biosolid	1	1.71	0.47	0.13	0.03

$$\mathrm{HHV\ (kJ/kg)} = 87352 \times \left(\frac{\mathrm{C}}{3} + \mathrm{H} + \frac{\mathrm{S}}{8}\right) \quad (1)$$

where C, H, and S are the weight percentages of carbon, hydrogen, and sulfur on a dry basis, respectively.

The lower heating value (LHV) has a relation with HHV and is shown in eq 2[33]

$$\mathrm{LHV\ (kJ/kg)} = \mathrm{HHV} - 2443 \times 8.936 \times \mathrm{H} \quad (2)$$

where 2443 kJ/kg is the latent heat of vaporization of water and 8.936 kg/kg is the ratio of water to hydrogen.

The specific chemical exergy of biosolid on a dry basis can be calculated according to its components as eq 3[25,34]

$$\mathrm{Ex_{ch,db}(kJ/kg)} = 36343.9\mathrm{C} + 107563.3\mathrm{H} - 8630.8\mathrm{O} + 414.7\mathrm{N} + 19079.8\mathrm{S} - 2110\mathrm{ash} \quad (3)$$

where C, H, O, N, S, and ash are the weight percent of the elements carbon, hydrogen, oxygen, nitrogen, and sulfur and ash on a dry basis, respectively.

As the reaction extent is assumed, the unreacted dry biosolid has to be heated to the reaction temperature. Since there is only a temperature change for the unreacted dry biosolid, its heat capacity C_P is important. The heat capacity of the dry biosolid is described as eq 4[35]

$$C_{P,\mathrm{dry\ biosolid}}\ (\mathrm{kJ/kg{\cdot}K}) = 1.5 + 0.001T \quad (4)$$

where T is the temperature (K) of the biomass.

The heat capacity of ash generated from the reacted biosolid is assumed as eq 5[36]

$$C_{P,\mathrm{ash}}\ (\mathrm{kJ/kg{\cdot}K}) = 0.84 \quad (5)$$

2.2. Basic Thermochemical Database. Table 5 shows the standard enthalpy (H_0), standard Gibbs free energy (G_0), standard chemical exergy ($\mathrm{Ex_{ch}}$), and coefficients (a, b, c, and d) of specific heat capacity (C_P) for an ideal gas at 1 atm (1.01325 bar) and 298.15 K (25 °C).

The LHV of the dry syngas in MJ/Nm^3 is calculated as eq 6[38]

$$\mathrm{LHV(syngas)\ (MJ/Nm^3)} = 10.8x_{\mathrm{H_2}} + 12.6x_{\mathrm{CO}} + 35.8x_{\mathrm{CH_4}} \quad (6)$$

where $X_{\mathrm{H_2}}$, X_{CO}, and $X_{\mathrm{CH_4}}$ are the mole fractions of H_2, CO, and CH_4 in the syngas, respectively.

Table 5. Thermochemical Properties of Gasification-Related Compounds[33a]

	H_0	G_0	$\mathrm{Ex_{ch}}$	C_P (kJ/(kmol K))				T range
Molecular	kJ/kmol	kJ/kmol	kJ/kmol	*a*	*b*	*c*	*d*	K
H_2	0	0	236,100	29.11	−0.001916	4.003×10^{-6}	-0.8704×10^{-9}	273−1800
CO	−110,530	−137,150	275,100	28.16	0.001675	5.372×10^{-6}	-2.222×10^{-9}	273−1800
CO_2	−393,520	−394,360	19,870	22.26	0.05981	-3.501×10^{-5}	7.469×10^{-9}	273−1800
H_2O (v)	−241,820	−228,590	9500	32.24	0.001923	1.055×10^{-5}	-3.595×10^{-9}	273−1800
CH_4	−74,850	−50,790	831,650	19.89	0.05024	1.269×10^{-5}	-11.01×10^{-9}	273−1500
N_2	0	0	720	28.9	−0.001571	8.081×10^{-6}	-2.873×10^{-9}	273−1800
H_2S	−19,960		812,000	29.6	0.0131	5.711×10^{-6}	-3.294×10^{-9}	273−1800
C_6H_6	82,930	129,660	3,303,600	−36.22	0.48475	-31.57×10^{-5}	77.62×10^{-9}	273−1500
C (s)	0	0	410,260	4.762	0.03148	-2.115×10^{-5}	5.717×10^{-9}	500−1500
O_2	0	0	3970					
H_2O (l)	−285,830	−237,180	900					

[a]Source: B.G. Kyle, Chemical and Process Thermodynamics (Englewood Cliffs, NJ: Prentice-Hall,1984); JANAF, Thermochemical Tables (Midland, MI: Dow Chemical Co., 1971). The C_P of char is generated from[37] $\left(4.03 + 1.14 \times 10^{-3}\,T - \frac{2.04 \times 10^5}{T^2}\right) \cdot 4.18\ \mathrm{J/(mol{\cdot}K)}$.

https://doi.org/10.1021/acsomega.4c01687
ACS Omega 2024, 9, 32639−32650

Without considering heat recovery, the CGE is calculated from

$$\text{CGE \%} = \frac{\text{LHV of syngas}}{\text{LHV of total biosolid}} \times 100\% \quad (7)$$

2.3. Equilibrium Constant *K* Calculation. The thermodynamic relationship between Gibbs free energy and equilibrium constants is shown

$$\Delta G = -RT\ln K = \Delta(H - TS) \quad (8)$$

where H and S are the enthalpy and entropy of a material at a given temperature and pressure, respectively.

The equilibrium constant has a relationship with enthalpy and entropy, which can be calculated from the heat capacity. The heat capacity is defined as

$$C_P = a + bT + cT^2 + dT^3 \quad (9)$$

where (T in K, C_P in kJ/(kmol·K)) a, b, c, and d are the constant coefficients of species and can be found in Table 5. Enthalpy change can be calculated from eq 10.

$$\Delta H = \int_{T_0}^{T} C_P dT \quad (10)$$

Integrating eq 10

$$H - H_0 = a(T - T_0) + \frac{b}{2}(T^2 - T_0^2) + \frac{c}{3}(T^3 - T_0^3) + \frac{d}{4}(T^4 - T_0^4) \quad (11)$$

Then

$$H = aT + \frac{b}{2}T^2 + \frac{c}{3}T^3 + \frac{d}{4}T^4 + \left(H_0 - aT_0 - \frac{b}{2}T_0^2 - \frac{c}{3}T_0^3 - \frac{d}{4}T_0^4\right) \quad (12)$$

G and H also have the relationship shown in eqs 13 or 14.

$$\frac{\partial\left(\frac{G}{RT}\right)}{\partial T} = -\frac{H}{RT^2} \quad (13)$$

$$\Delta\left(\frac{G}{T}\right) = \int_{T_0}^{T} -\frac{H}{T^2} dT \quad (14)$$

Integrating eq 14

$$\frac{G}{T} - \frac{G_0}{T_0} = -a(\ln T - \ln T_0) - \frac{b}{2}(T - T_0) - \frac{c}{3}\left(\frac{1}{2}T^2 - \frac{1}{2}T_0^2\right) - \frac{d}{4}\left(\frac{1}{3}T^3 - \frac{1}{3}T_0^3\right) + \left(H_0 - aT_0 - \frac{b}{2}T_0^2 - \frac{c}{3}T_0^3 - \frac{d}{4}T_0^4\right)\frac{1}{T} - \left(\frac{H_0}{T_0} - a - \frac{b}{2}T_0 - \frac{c}{3}T_0^2 - \frac{d}{4}T_0^3\right) \quad (15)$$

Then

$$\frac{G}{T} = -a\ln T - \frac{b}{2}T - \frac{c}{6}T^2 - \frac{d}{12}T^3 + \left(H_0 - aT_0 - \frac{b}{2}T_0^2 - \frac{c}{3}T_0^3 - \frac{d}{4}T_0^4\right)\frac{1}{T} + \left(\frac{G_0 - H_0}{T_0} + a(1 + \ln T_0) + bT_0 + \frac{c}{2}T_0^2 + \frac{d}{3}T_0^3\right) \quad (16)$$

The enthalpy of formation, Gibbs function of formation, and ideal-gas specific heats of the gases are all functions of temperature. From eq 8

$$\ln K = -\frac{\sum_i \nu_i G_i}{RT} \quad (17)$$

where ν_i is the stoichiometric number, positive for products and negative for reactants.

Tar includes one-ring, two-ring, and three-ring aromatic hydrocarbons and phenolic, etc., and benzene (C_6H_6) is always used as a typical compound for tar.[39] The four reactions employed are the water gas shift (WGS) reaction ($K1$), methane steam reforming reaction ($K2$), Boudouard reaction ($K3$), and benzene generation reaction ($K4$) as follows

$$CO + H_2O{=}CO_2 + H_2 \quad (K1)$$

$$K1 = \frac{[CO_2][H_2]}{[CO][H_2O]} = \frac{x_{CO_2}x_{H_2}}{x_{CO}x_{H_2O}} \quad (18)$$

$$CH_4 + H_2O{=}CO + 3H_2 \quad (K2)$$

$$K2 = \frac{[CO][H_2]^3}{[CH_4][H_2O]} = \frac{x_{CO}x_{H_2}^3}{x_{CH_4}x_{H_2O}}\left(\frac{P}{P_0}\right)^2 \quad (19)$$

$$C\ (s) + CO_2{=}2CO \quad (K3)$$

$$K3 = \frac{[CO]^2}{[CO_2]} = \frac{x_{CO}^2}{x_{CO_2}} \times \frac{P}{P_0} \quad (20)$$

$$6CO + 9H_2{=}C_6H_6 + 6H_2O \quad (K4)$$

$$K4 = \frac{[C_6H_6][H_2O]^6}{[CO]^6[H_2]^9} = \frac{x_{C_6H_6}x_{H_2O}^6}{x_{CO}^6 x_{H_2}^9}\left(\frac{P_0}{P}\right)^8 \quad (21)$$

where P_0 is the pressure of the standard condition and P is the real pressure.

Thermodynamic equilibrium constants are a function of temperature. The values of $K1$, $K2$, $K3$, and $K4$ can be obtained after plugging the H_0, a, b, c, and d values of the heat capacity of each component and the stoichiometric number of the four reactions into eq 17. The stoichiometric numbers of the four equations are shown in Table 6.

$$\ln K1 = \frac{4871.41}{T} - 1.08612\ln T + 3.26534 \times 10^{-3} T - 0.940763 \times 10^{-6} T^2 + 1.24445 \times 10^{-10} T^3 + 0.502068 \quad (22)$$

https://doi.org/10.1021/acsomega.4c01687
ACS Omega 2024, 9, 32639−32650

$$\ln K2 = \frac{-22826.7}{T} + 7.62088\ln T - 3.38201 \times 10^{-3} T - 0.117452 \times 10^{-6} T^2 + 0.979452 \times 10^{-10} T^3 - 23.2215 \quad (23)$$

$$\ln K3 = \frac{-20095.9}{T} + 3.52394\ln T - 5.28867 \times 10^{-3} T + 1.34119 \times 10^{-6} T^2 - 1.76710 \times 10^{-10} T^3 + 0.351897 \quad (24)$$

$$\ln K4 = \frac{77326.8}{T} - 32.9240\ln T + 30.2792 \times 10^{-3} T - 6.42809 \times 10^{-6} T^2 + 7.73952 \times 10^{-10} T^3 + 88.7994 \quad (25)$$

Table 6. Stoichiometric Number of the Four Reactions

ν_i	C (s)	H_2	CO	CO_2	H_2O (v)	CH_4	C_6H_6 (v)
K1	0	1	−1	1	−1	0	0
K2	0	3	1	0	−1	−1	0
K3	−1	0	2	−1	0	0	0
K4	0	−9	−6	0	6	0	1

2.4. Exergy Analysis. The kinetic exergy and potential exergy are neglected in a thermodynamic system. Chemical exergy is needed for solution, in relation to fugacity. The chemical exergy is the amount of energy obtained, relative to its reference conditions. The reference environment is pointed to the standard conditions of 1 atm (1.01325 bar) and 298.15 K (25 °C) for pressure and temperature, respectively.

For the pure material, the exergy can be shown in eq 26.

$$\mathrm{Ex}(T, P) = \mathrm{Ex}(T_0, P_0) + H - H_0 - T_0(S - S_0) \quad (26)$$

where $\mathrm{Ex}(T_0, P_0)$ is the standard chemical exergy of a pure chemical species.

The enthalpy changes have been presented in the previous part, and the entropy changes can be calculated as eq 27.

$$\Delta S = S - S_0 = \int_{T_0}^{T} \frac{C_P}{T} dT - \int_{P_0}^{P} \frac{R}{P} dP \quad (27)$$

If there is no pressure change

$$\Delta S = \int_{T_0}^{T} \frac{C_P}{T} dT \quad (28)$$

The exergy content for a stream with independent variables, including temperature (T), pressure (P), and composition (x), is shown in eq 29

$$\mathrm{Ex}(T, P, x) = \sum x_i\{\mathrm{Ex}_i(T, P) + RT_0 \ln(x_i) + H_i^E - T_0 S_i^E\} \quad (29)$$

where the sub-index "i" indicates component i in the stream. Superscript E indicates the excess property.

If the components are in ideal conditions, eq 29 is simplified to eqs 30 or 31

$$\mathrm{Ex}(T, P, x) = \sum x_i\{\mathrm{Ex}_i(T, P) + RT_0 \ln(x_i)\} \quad (30)$$

$$x(T, P, x) = \sum x_i\{\mathrm{Ex}_i(T_0, P_0) + H_i - H_{i,0} - T_0(S_i - S_{i,0}) + RT_0\ln(x_i)\} \quad (31)$$

Therefore, the total exergy of each stream, consisting of physical exergy (Ex_{ph}) and chemical exergy (Ex_{ch}), can be determined. The physical exergy refers to the amount of usable energy without chemical compositions and is expressed as[33]

$$\mathrm{Ex}_i(T, P)_{ph} = H_i - H_{i,0} - T_0(S_i - S_{i,0}) \quad (32)$$

Chemical exergy is expressed as[33]

$$\mathrm{Ex}_i(T, P, x_i)_{ch} = \mathrm{Ex}_i(T_0, P_0) + RT_0 \ln(x_i) \quad (33)$$

where T_0 and P_0 are the temperature and pressure of the reference state, x_i is the mole fraction of a pure chemical species i in the mixture, and R is the molar gas constant.

Exergy efficiency is the ratio of the total exergy of the outlet stream to the total exergy of the inlet stream

$$H_{Ex}\,\% = \frac{\mathrm{Ex}_{out}}{\mathrm{Ex}_{in}} \times 100\% \quad (34)$$

Ex_{out} and Ex_{in} represent the sum of the exergies of outputs and the sum of the exergies of inputs, respectively. The outlet exergy includes the exergies in the product gas, char, ash, and unreacted dry biosolid. The inlet exergy includes the exergies in total dry biosolid and its accompanied moisture and gasification agents.

3. THERMODYNAMICS EQUILIBRIUM MODEL PROCESS FOR BIOSOLID GASIFICATION

3.1. Equations of the Thermodynamic Equilibrium Model. Biosolid gasification is assumed to occur under these conditions: Based on 1 mol of $CH_wO_xN_yS_z$, a few unreacted dry biosolids, consisting of organic material and ash, retained their original organic composition, benzene (C_6H_6) was used as a typical compound for tar; reaching equilibrium; under atmosphere pressure; syngas was assumed as an ideal gas.

The gasifying agents are air (or pure oxygen), steam, and carbon dioxide. The influent and effluent of biosolid gasification are depicted in Figure 3.

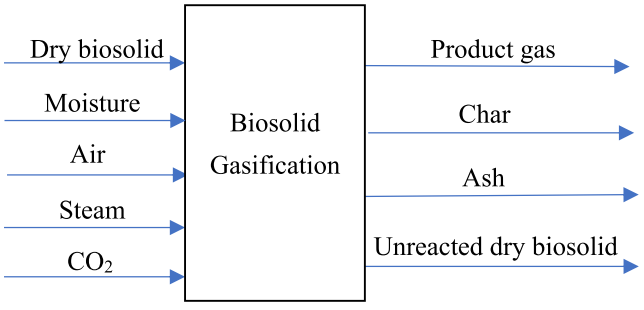

Figure 3. Influent and effluent diagram of biosolid gasification.

The stoichiometric equilibrium model is based on MESH equations (material balance equations, phase equilibrium equations, mole fraction summation equations, and heat, which means energy balance equations). The typical global gasification reaction can be written as follows

https://doi.org/10.1021/acsomega.4c01687
ACS Omega 2024, 9, 32639−32650

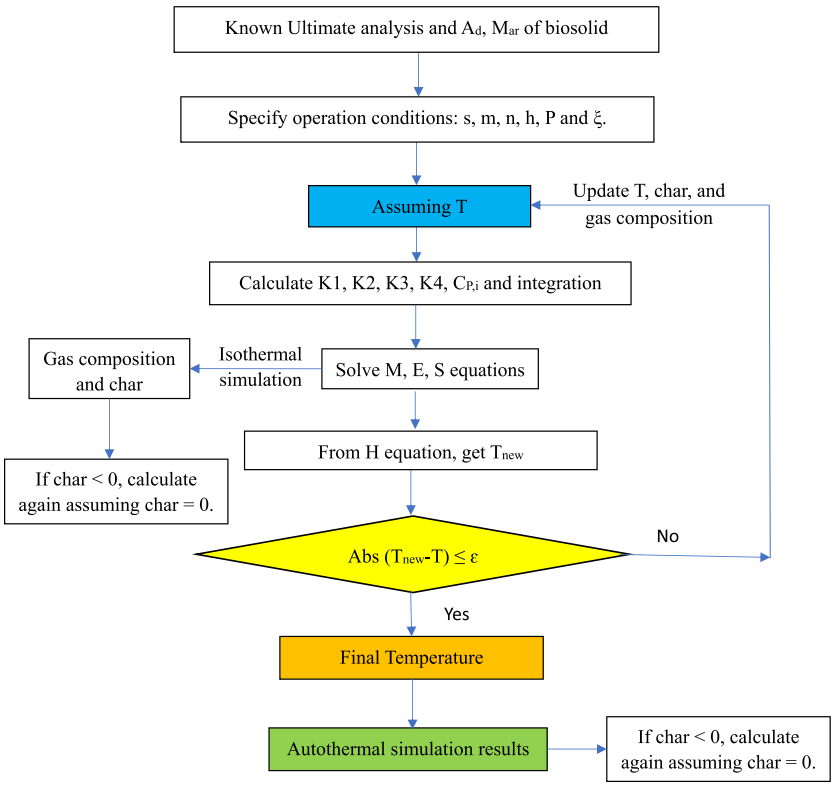

Figure 4. Calculation procedure of the stoichiometric equilibrium model.

$$(CH_wO_xN_yS_z + M_{ash} + wH_2O(l)) + sH_2O(steam) + mO_2 + m\cdot\left(\frac{1}{mc} - 1\right)\cdot N_2 hCO_2 = x_{H_2} + x_{CO} + x_{CO_2} + x_{H_2O} + x_{CH_4} + x_{N_2} + x_{H_2S} + x_{C_6H_6})\cdot N_g + N_C + \xi\cdot M_{ash}$$
$$(1 - \xi)\cdot(CH_wO_xN_yS_z + M_{ash}) \quad (35)$$

where w, x, y, and z are hydrogen, oxygen, nitrogen, and sulfur atoms per atom of carbon in the biosolid, respectively; w refers to moles of moisture per mol of biosolid; m refers to moles of oxygen supplied per mole of biosolid; mc is the oxygen concentration in the supplied air; N_g is the total mole of the gas mixture; ξ is the conversion of the biosolid; N_C is the mole of char; and M_{ash} is the mass of ash.

The oxygen supplied in gasification is calculated in eq 36

$$m = (\text{oxygen})_{\text{stoichiometric}} \times \text{equivalence ratio} \quad (36)$$

where stoichiometric oxygen is the oxygen required for complete combustion of the biosolid.

There are 11 unknowns required to find their values: X_{H_2}, X_{CO},X_{CO_2}, X_{H_2O}, X_{CH_4}, X_{N_2}, X_{H_2S}, $X_{C_6H_6}$, N_g, N_C, and temperature. Meanwhile, there are five equations obtained from the five elemental molar balances (carbon, hydrogen, oxygen, nitrogen, and sulfur)

$$\text{carbon molar balance: } (x_{CO} + x_{CO_2} + x_{CH_4} + 6x_{C_6H_6})\cdot N_g + N_C = \xi + h \quad (37)$$

$$\text{hydrogen molar balance: } (2x_{H_2} + 2x_{H_2O} + 4x_{CH_4} + 2x_{H_2S} + 6x_{C_6H_6})\cdot N_g = a\cdot\xi + 2w + 2s \quad (38)$$

$$\text{oxygen molar balance: } (x_{CO} + 2x_{CO_2} + x_{H_2O})\cdot N_g = b\cdot\xi + w + s + 2m + 2h \quad (39)$$

$$\text{nitrogen molar balance: } 2x_{N_2}\cdot N_g = c\cdot\xi + 2m\cdot\left(\frac{1}{mc} - 1\right) \quad (40)$$

$$\text{sulfur molar balance: } x_{H_2S}\cdot N_g = d\cdot\xi \quad (41)$$

The one summation of mole fraction equation for the gas phase is

$$x_{H_2} + x_{CO} + x_{CO_2} + x_{H_2O} + x_{CH_4} + x_{N_2} + x_{H_2S} + x_{C_6H_6} = 1 \quad (42)$$

There are four equilibrium constant relations expressed in eq 18 for the water gas shift (WGS) reaction, eq 19 for the methane steam reforming reaction, eq 20 for the Boudouard reaction, and eq 21 for the benzene generation reaction.

One energy balance (heat) equation is the conversion of energy (adiabatic process)

https://doi.org/10.1021/acsomega.4c01687
ACS Omega 2024, 9, 32639−32650

$$H^0_{f,\text{drybiosolid}} + wH^0_{f,H_2O(l)} + sH^0_{f,H_2O(g)} + mH^0_{f,o_2} + m\cdot\left(\frac{1}{mc} - 1\right)H^0_{f,N_2} + hH^0_{f,CO_2} = N_g\left(\sum_1^8 x_i H^0_{f,i} + \int_{T_0}^{T}\sum_1^8 x_i C_{P,i}dT\right) + N_C\left(H^0_{f,C} + \int_{T_0}^{T} C_{P,\text{char}}dT\right) + (\xi\cdot M_{\text{ash}})\int_{T_0}^{T} C_{P,\text{ash}}dT + (1-\xi)\left(H^0_{f,\text{drybiosolid}} + \int_{T_0}^{T} C_{P,\text{drybiosolid}}dT\right) \quad (43)$$

where $H^0_{f,i}$ is the standard enthalpy of formation of species i; x_i represents the mole fraction of species i in the gas mixture; $C_{P,i}$ is the specific heat of species i in the gas mixture; the formation enthalpy of the dry biosolid is calculated through the HHV.

3.2. Calculation Procedure. The model can work under isothermal and autothermal conditions (self-sufficiency). The calculation procedure of the stoichiometric equilibrium model is illustrated in Figure 4. If the quantity of char in the final simulation results is negative, then the quantity of char will be put to zero and the simulation will be carried out again without the equilibrium constant K3.

4. RESULTS AND DISCUSSION

4.1. Model Validation. These simulation results consider four equilibrium constants under ER of 0.3 and 0.4 and a moisture content of 20% for woody gasification, and biosolid gasification is shown in Figure 5.

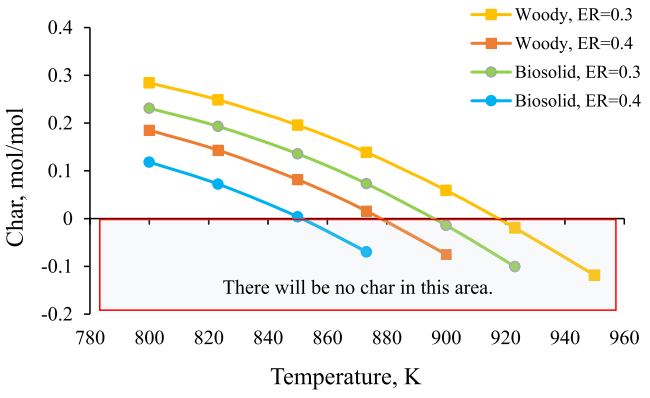

Figure 5. Simulation results considering four equilibrium constants.

From Figure 5, there will be char generation below a certain temperature at different conditions. If the amount of char is negative, it means that there will be no char formation, and the model will run again without considering the equilibrium constant $K3$.

The model was validated through comparison with the woody gasification results available in the literature. The conditions are a moisture content of 20% and held at a given temperature of 1073 K at atmosphere pressure. There will be no char formation, and the benzene concentration in the syngas is very low because of the very small equilibrium constant for the benzene generation reaction ($K4$). The result comparison is illustrated in Table 7.

From Table 7, the result for an ER of 0.3 is similar to those of the nonstoichiometric method, while the result for an ER of 0.4 is close to that for the stoichiometric method. Overall, this work agrees well with the experimental data. However, hydrogen production is always overestimated, and methane production is underestimated in the equilibrium model relative to the experiment results. This is mainly because the CH_4 reaction equilibrium is not achieved.

4.2. Temperature Influence under Isothermal Conditions on Biosolid Gasification. From Figure 5, there is no char formation in biosolid gasification when the temperature is above 900 K, with a moisture content of 20%, an ER of 0.3, a reaction extension of 100%, and under atmosphere pressure. The solved concentration result from biosolid gasification at different given temperatures from 900 to 1200 K (isothermal) is illustrated in Figure 6.

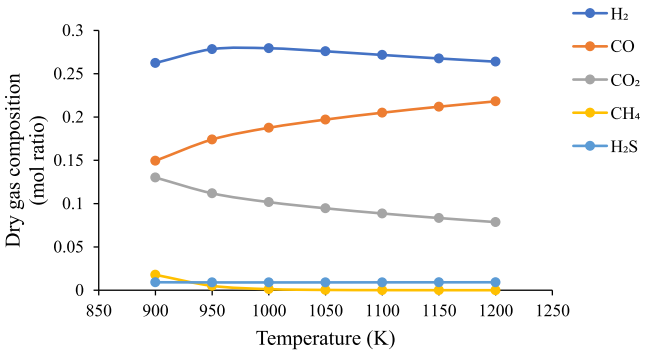

Figure 6. Concentrations at different given temperatures of biosolid gasification.

As the temperature increases, the CO concentration goes up while the CO_2 and CH_4 concentrations decrease continuously. The H_2 concentration of the dry syngas in biosolid gasification shows a curve against the given temperature, and the maximum

Table 7. Comparison of Different Models on Product Gas Component Distribution

	real	equilibrium model		this work	
	experimental[31] (%)	nonstoichiometric[33] (%)	stoichiometric[40] (%)	ER of 0.3 (%)	ER of 0.4 (%)
H_2	15.23	25.35	18.44	25.49	19.96
CO	23.04	23.73	17.46	24.06	18.77
CO_2	16.42	10.54	13.13	10.43	12.67
CH_4	1.58	0.02	0.00	0.02	0.01
N_2	42.31	40.36	50.96	40.00	48.60
O_2	1.42	0	0	0	0
Total	100	100	100	100	100

https://doi.org/10.1021/acsomega.4c01687
ACS Omega 2024, 9, 32639−32650

concentration reaches around 973 K. Before 973 K, more CH_4 is converted to H_2 as temperature increases; after 973 K, more H_2 is converted to H_2O as temperature increases.

4.3. Design of Experiment under Autothermal Conditions. The four factors and their corresponding levels in the design of experiment (DOE) are illustrated in Table 8, and there are 24 = 16 rounds. The total 16 rounds of modeling results are illustrated in Table S1 in the Supporting Information.

Table 8. DOE of Autothermal Biosolid Gasification

factors	level (−1)	level (+1)
feedstock	woody	biosolid
moisture content	10%	20%
ER	0.3	0.4
reaction extension	100%	90%

From Table S1, under autothermal conditions, there is no case of char generation in woody gasification; while there is char generation in biosolid gasification when the ER is 0.3, but there is no char when the ER is 0.4. A Pareto chart of the effects of adiabatic temperature (α = 0.05) is shown in Figure 7, and the effects of the four factors on adiabatic temperature are illustrated in Figure 8.

Figure 7 indicates that the four factors are all the main factors for adiabatic temperature. As shown in Figure 8, the adiabatic temperature correlates significantly with the feedstock type, moisture content, ER, and reaction extent. Biosolid gasification has a lower adiabatic temperature than woody gasification as it has lower HHV. The moisture in the biosolid, unlike steam as an agent, has to evaporate first at the start of the gasification process. The higher the water content in the biosolid, the more the energy required to evaporate it, so the lower the adiabatic temperature. However, water can participate in the water gas shift reaction instead of the steam feed. The adiabatic temperature increases when the ER is higher as more energy is released from the feedstock. When the reaction extension is lower, ER is relatively higher for the reacted feedstock than the designed ER, so the adiabatic temperature is higher, but both the amount and LHV of dry syngas are lower.

A Pareto chart of the effects of exergy efficiency (α = 0.05) is shown in Figure 9, and the effects of the four factors on exergy efficiency are illustrated in Figure 10.

Figure 9 indicates that the four factors are all also the main factors for exergy efficiency. From Figure 10, the feedstock type has a minor effect on the exergy efficiency. The ER is the most influential parameter on the exergy efficiency because the reaction itself destroys most exergy. If the reaction extension is not 100%, some biosolids are not converted to syngas, and they still retain their original exergy; then the process has higher exergy efficiency.

The main effect plots for moles of dry syngas, H_2 concentration, CO concentration, CH_4 concentration, and CGE are illustrated in Figure 11.

As shown in Figure 11, biosolid gasification needs more air than woody gasification at the same ER because its stoichiometric air is higher than that of woody gasification, so it produces more dry syngas. The other three factors also positively affect the moles of dry syngas. As there is char generation in some cases of biosolid gasification, the syngas of biosolid gasification has a lower CO concentration than that of woody gasification, which impacts further utilization. A higher ER generates more dry syngas and lowers the H_2 and CH_4 concentrations while raising the CO concentration. The reaction extension increases not only the moles of dry syngas but also the concentration of H_2, CO, and CH_4. According to Table S1, the LHV of dry syngas ranges from 3.64 to 5.90 MJ/Nm^3, which is the normal value of dry syngas from air gasification. If the reaction extension is not 100%, some biosolids are not converted to syngas, so the amount and LHV of dry syngas and CGE are lower.

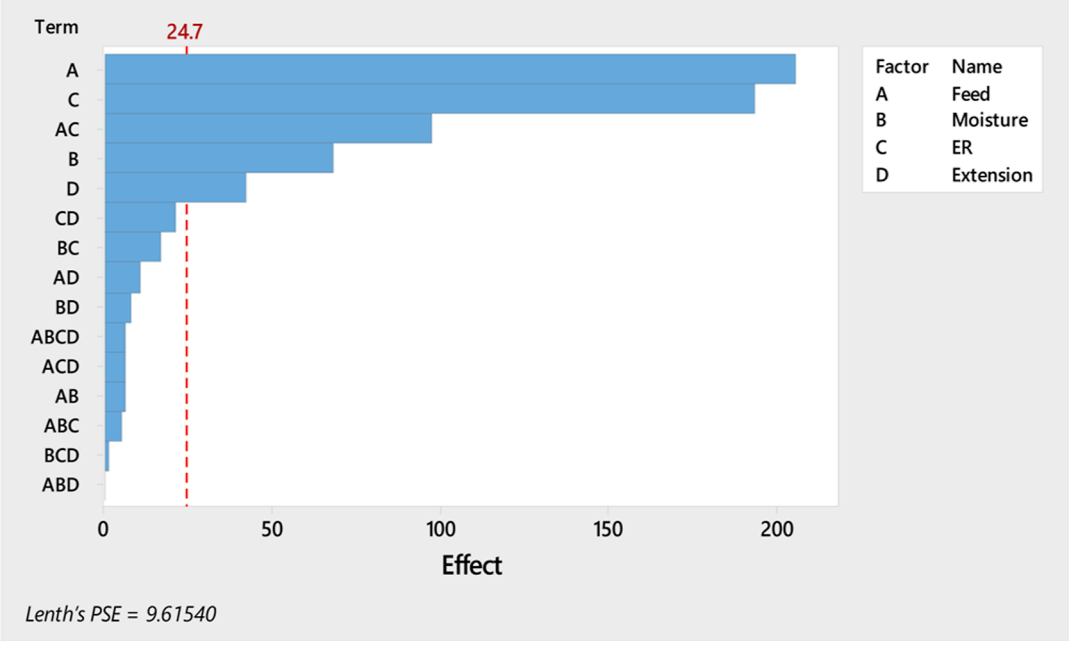

Figure 7. Pareto chart of the effects for adiabatic temperature (α = 0.05).

https://doi.org/10.1021/acsomega.4c01687
ACS Omega 2024, 9, 32639−32650

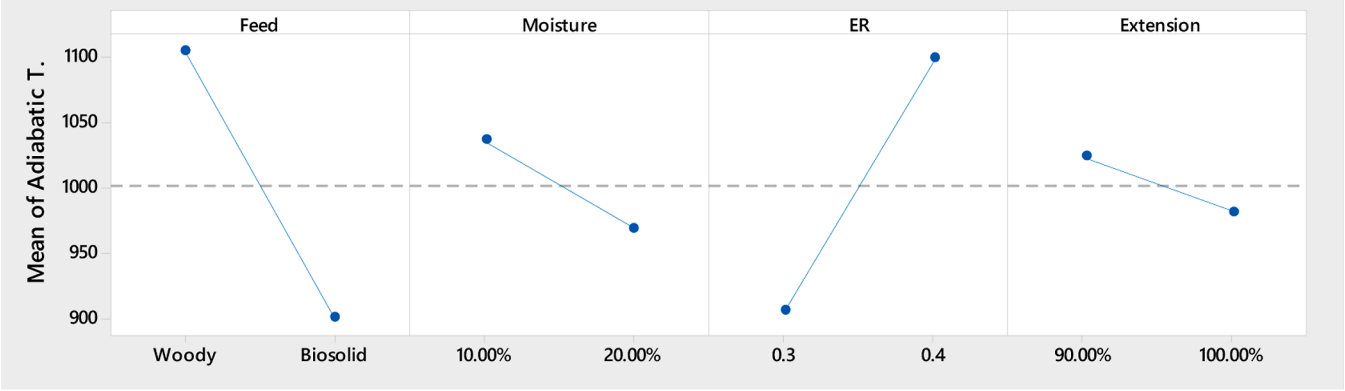

Figure 8. Main effect plots for the adiabatic temperature.

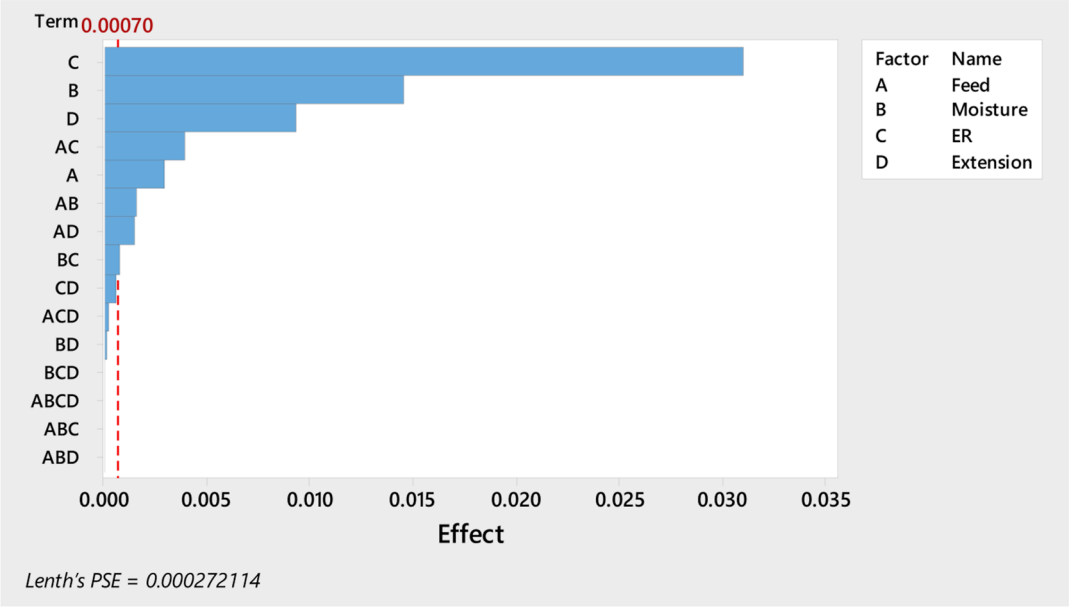

Figure 9. Pareto chart of the effects for exergy efficiency (α = 0.05).

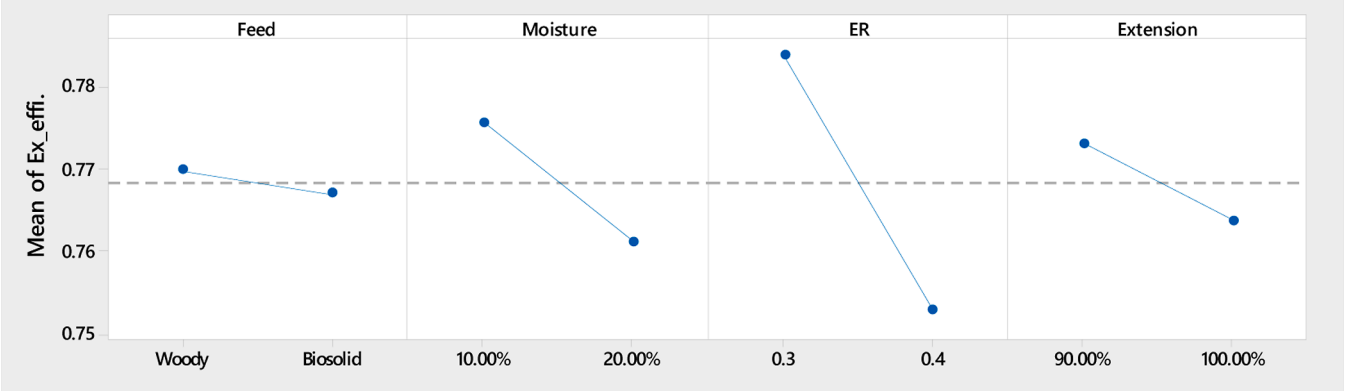

Figure 10. Main effect plots for exergy efficiency.

4.4. Effect of Moisture Content. There is no char generation when the moisture content ranges from 10 to 40% for both woody gasification and biosolid gasification at an ER of 0.4 and the reaction extent is 100%. The effect of moisture content on the autothermal temperature is illustrated in Figure 12.

The temperature decreases continuously with moisture from 10 to 40% for both woody gasification and biosolid gasification, and the biosolid gasification autothermal temperature is lower than the temperature of woody gasification. The effect of the moisture content on the exergy efficiency is illustrated in Figure 13.

https://doi.org/10.1021/acsomega.4c01687
ACS Omega 2024, 9, 32639−32650

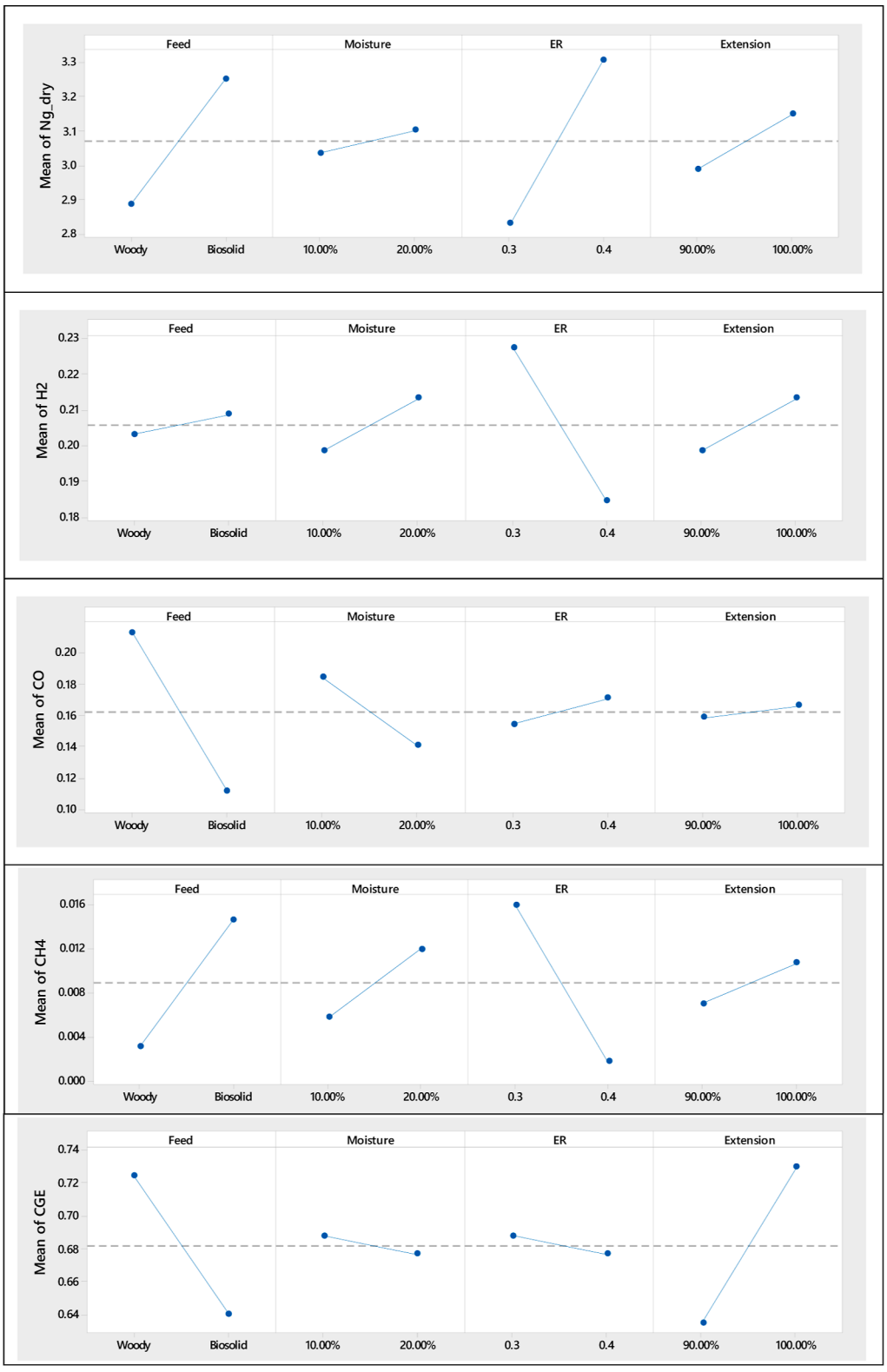

Figure 11. Main effect plots for moles of dry syngas and concentrations of H_2, CO, CH_4, and CGE.

Woody gasification and biosolid gasification have similar exergy efficiencies under these cases, and both decrease with moisture. Variation of dry syngas composition for H_2, CO, CO_2, and CH_4 against moisture content in biosolid gasification is illustrated in Figure 14.

The difference in the chemical compositions of the feedstocks significantly affects the main components. The CH_4 concentration has a strong correlation with the adiabatic temperature. An increase in moisture leads to an increase in CH_4 due to the temperature decrease. The H_2 concentration shows a curve against the moisture content of the biosolid. More moisture provides more hydrogen sources in the reaction, but the autothermal temperature drops and more H_2 is converted to CH_4.

https://doi.org/10.1021/acsomega.4c01687
ACS Omega 2024, 9, 32639−32650

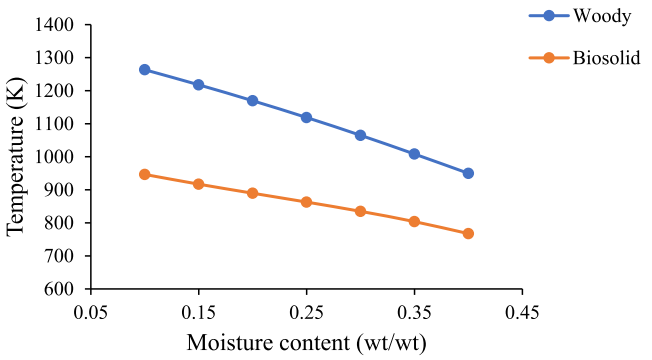

Figure 12. Effect of moisture content on the autothermal temperature under ER = 0.4.

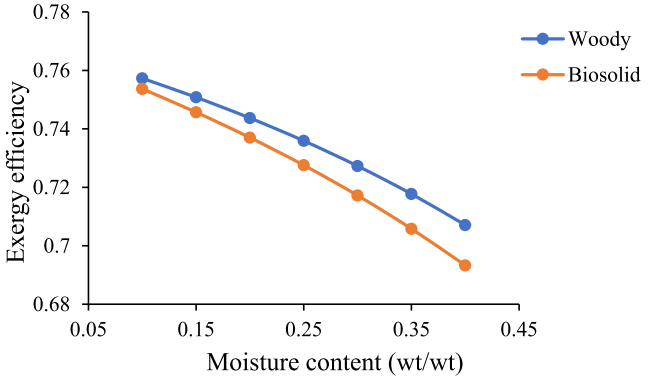

Figure 13. Effect of moisture content on exergy efficiency under ER = 0.4.

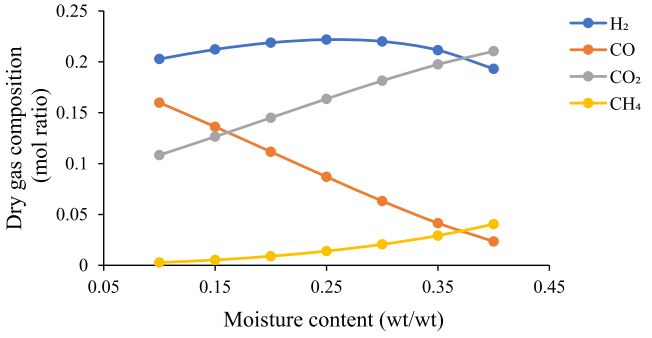

Figure 14. Effect of moisture content of the biosolid on syngas concentration at ER = 0.4.

5. CONCLUSIONS

Biosolid gasification is a promising method of sludge to energy technology. A stoichiometric thermodynamic equilibrium model was developed to simulate the biosolid gasification process based on the biosolid properties, thermodynamic database, and equilibrium constants to optimize the energy recovery from biosolids generated in wastewater treatment. If the calculation result showed that the quantity of char was negative, the char was not considered in the following simulation. It had a good agreement with woody gasification under isothermal conditions, and the influence of a given temperature on biosolid gasification was simulated. Then, the study explored the effects of the feedstock, moisture content, ER, and reaction extension on the adiabatic temperature, exergy efficiency, and syngas properties under autothermal conditions. The four factors are all main factors for the adiabatic temperature. The exergy efficiency depended more on the operation conditions than the feedstock type. The H_2 concentration of the dry syngas in biosolid gasification exhibited a curve both against the given temperature under isothermal conditions and against the moisture content under autothermal conditions. The model can be used to guide the development and design of the biosolid gasification process.

■ ASSOCIATED CONTENT

Supporting Information

The Supporting Information is available free of charge at https://pubs.acs.org/doi/10.1021/acsomega.4c01687.

Woody gasification and biosolid gasification modeling results including moisture content, H_2, CO, CO_2, CH_4, N_2 contents, etc. (PDF)

■ AUTHOR INFORMATION

Corresponding Author

Yun Ji − *Department of Chemical Engineering, University of North Dakota, Grand Forks, North Dakota 58202, United States;* orcid.org/0000-0003-0754-5321; Email: yun.ji@engr.und.edu

Authors

Fangtian Li − *Department of Chemical Engineering, University of North Dakota, Grand Forks, North Dakota 58202, United States*

Xin Zhang − *Department of Chemical Engineering, University of North Dakota, Grand Forks, North Dakota 58202, United States*

Complete contact information is available at: https://pubs.acs.org/10.1021/acsomega.4c01687

Notes

The authors declare no competing financial interest.

■ ACKNOWLEDGMENTS

The authors would like to acknowledge the financial support from the City of Grand Forks, North Dakota. The authors also would like to thank the Grand Forks Wastewater Treatment Plant, AE2S, and the University of North Dakota for their technical support.

■ REFERENCES

(1) Safarian, S.; Unnthorsson, R.; Richter, C. Performance Investigation of Biomass Gasification for Syngas and Hydrogen Production Using Aspen Plus. *Open J. Model. Simulat.* **2022**, *10*, 71−87.

(2) Paz-Ferreiro, J.; Nieto, A.; Méndez, A.; Askeland, M.; Gascó, G. Biochar from Biosolids Pyrolysis: A Review. *Int. J. Environ. Res. Publ. Health* **2018**, *15* (5), 956.

(3) Hu, M.; Ye, Z.; Zhang, H.; Chen, B.; Pan, Z.; Wang, J. Thermochemical Conversion of Sewage Sludge for Energy and Resource Recovery: Technical Challenges and Prospects. *Environ. Pollut. Bioavailability* **2021**, *33* (1), 145−163.

(4) Bora, R. R.; Richardson, R. E.; You, F. Resource Recovery and Waste-to-Energy from Wastewater Sludge via Thermochemical Conversion Technologies in Support of Circular Economy: A Comprehensive Review. *BMC Chem. Eng.* **2020**, *2* (1), 8.

(5) Oladejo, J.; Shi, K.; Luo, X.; Yang, G.; Wu, T. A Review of Sludge-to-Energy Recovery Methods. *Energies* **2018**, *12* (1), 60.

(6) Gao, N.; Kamran, K.; Quan, C.; Williams, P. T. Thermochemical Conversion of Sewage Sludge: A Critical Review. *Prog. Energy Combust. Sci.* **2020**, *79*, 100843.

(7) Kacprzak, M.; Neczaj, E.; Fijałkowski, K.; Grobelak, A.; Grosser, A.; Worwag, M.; Rorat, A.; Brattebo, H.; Almås, Å.; Singh, B. R. Sewage Sludge Disposal Strategies for Sustainable Development. *Environ. Res.* **2017**, *156*, 39−46.
(8) Hla, S. S.; Sujarittam, N.; Ilyushechkin, A. Thermochemical Conversion Characteristics of Biosolid Samples from a Wastewater Treatment Plant in Brisbane, Australia. *Environ. Chem.* **2023**, *19* (6), 385−399.
(9) Moon, J.; Mun, T.-Y.; Yang, W.; Lee, U.; Hwang, J.; Jang, E.; Choi, C. Effects of Hydrothermal Treatment of Sewage Sludge on Pyrolysis and Steam Gasification. *Energy Convers. Manage.* **2015**, *103*, 401−407.
(10) Quan, L. M.; Kamyab, H.; Yuzir, A.; Ashokkumar, V.; Hosseini, S. E.; Balasubramanian, B.; Kirpichnikova, I. Review of the Application of Gasification and Combustion Technology and Waste-to-Energy Technologies in Sewage Sludge Treatment. *Fuel* **2022**, *316*, 123199.
(11) Arena, U. Process and Technological Aspects of Municipal Solid Waste Gasification. A Review. *Waste Manage.* **2012**, *32* (4), 625−639.
(12) International Biochar Initiative. *IBI White Paper: Pyrolysis and Gasification of Biosolids to Produce Biochar*; IBI, 2013.
(13) Abdelrahim, A.; Brachi, P.; Ruoppolo, G.; Fraia, S. D.; Vanoli, L. Experimental and Numerical Investigation of Biosolid Gasification: Equilibrium-Based Modeling with Emphasis on the Effects of Different Pretreatment Methods. *Ind. Eng. Chem. Res.* **2020**, *59* (1), 299−307.
(14) De Buck, V.; Polanska, M.; Van Impe, J. Modeling Biowaste Biorefineries: A Review. *Front. Sustain. Food Syst.* **2020**, *4*, 11.
(15) Ajorloo, M.; Ghodrat, M.; Scott, J.; Strezov, V. Recent Advances in Thermodynamic Analysis of Biomass Gasification: A Review on Numerical Modelling and Simulation. *J. Energy Inst.* **2022**, *102*, 395−419.
(16) Silva, I. P.; Lima, R. M. A.; Santana, H. E. P.; Silva, G. F.; Ruzene, D. S.; Silva, D. P. Development of a Semi-Empirical Model for Woody Biomass Gasification Based on Stoichiometric Thermodynamic Equilibrium Model. *Energy* **2022**, *241*, 122894.
(17) Tay, D. H. S.; Kheireddine, H.; Ng, D. K. S.; El-Halwagi, M. M.; Tan, R. R. Conceptual Synthesis of Gasification-Based Biorefineries Using Thermodynamic Equilibrium Optimization Models. *Ind. Eng. Chem. Res.* **2011**, *50* (18), 10681−10695.
(18) Agu, C. E.; Pfeifer, C.; Eikeland, M.; Tokheim, L.-A.; Moldestad, B. M. E. Detailed One-Dimensional Model for Steam-Biomass Gasification in a Bubbling Fluidized Bed. *Energy Fuels* **2019**, *33* (8), 7385−7397.
(19) von Berg, L.; Anca-Couce, A.; Hochenauer, C.; Scharler, R. Multi-Scale Modelling of Fluidized Bed Biomass Gasification Using a 1D Particle Model Coupled to CFD. *Fuel* **2022**, *324*, 124677.
(20) Baruah, D.; Baruah, D. C. Modeling of Biomass Gasification: A Review. *Renew. Sustain. Energy Rev.* **2014**, *39*, 806−815.
(21) Safarian, S.; Unnpórsson, R.; Richter, C. A Review of Biomass Gasification Modelling. *Renew. Sustain. Energy Rev.* **2019**, *110*, 378−391.
(22) Zainal, Z. A.; Ali, R.; Lean, C. H.; Seetharamu, K. N. Prediction of performance of a downdraft gasifier using equilibrium modeling for different biomass materials. *Energy Convers. Manage.* **2001**, *42*, 1499−1515.
(23) Sharma, S.; Sheth, P. N. Air-Steam Biomass Gasification: Experiments, Modeling and Simulation. *Energy Convers. Manage.* **2016**, *110*, 307−318.
(24) Jarungthammachote, S.; Dutta, A. Thermodynamic Equilibrium Model and Second Law Analysis of a Downdraft Waste Gasifier. *Energy* **2007**, *32* (9), 1660−1669.
(25) Shahbeig, H.; Shafizadeh, A.; Rosen, M. A.; Sels, B. F. Exergy Sustainability Analysis of Biomass Gasification: A Critical Review. *Biofuel Res. J.* **2022**, *9* (1), 1592−1607.
(26) Cohce, M. K.; Dincer, I.; Rosen, M. A. Energy and Exergy Analyses of a Biomass-Based Hydrogen Production System. *Bioresour. Technol.* **2011**, *102* (18), 8466−8474.
(27) Jiao, L.; Li, J.; Yan, B.; Chen, G.; Ahmed, S. Microwave Torrefaction Integrated with Gasification: Energy and Exergy Analyses Based on Aspen Plus Modeling. *Appl. Energy* **2022**, *319*, 119255.
(28) Li, D.; Liu, J.; Wang, S.; Cheng, J. Study on Coal Water Slurries Prepared from Coal Chemical Wastewater and Their Industrial Application. *Appl. Energy* **2020**, *268*, 114976.
(29) Wilmer, J.; Seames, W.; Bazile, D.; Smith, K. L.; Koster, B.; Mauch, G.; Weimer, L. Evaluating the Technical and Economic Feasibility of Adding a Power Recovery System to the Steam Condenser of a Lignite Coal-Fired Power Plant. *J. Power Energy Eng.* **2022**, *10* (11), 16−34.
(30) Galbreath, K. C. *Subtask 2.1—Effects of Cofiring Lignin and Biosolids with Coal on Fireside Performance and Combustion Products*; Energy & Environmental Research Center, University of North Dakota, 2002; p 54.
(31) Alauddin, Z. A. Z. Performance and Characteristics of a Biomass Gasifier System. PhD Thesis, University of Wales College of Cardiff, UK, 1996.
(32) Qian, H.; Guo, X.; Fan, S.; Hagos, K.; Lu, X.; Liu, C.; Huang, D. A Simple Prediction Model for Higher Heat Value of Biomass. *J. Chem. Eng. Data* **2016**, *61* (12), 4039−4045.
(33) Caglar, B.; Tavsanci, D.; Biyik, E. Multiparameter-Based Product, Energy and Exergy Optimizations for Biomass Gasification. *Fuel* **2021**, *303*, 121208.
(34) Song, G.; Xiao, J.; Zhao, H.; Shen, L. A Unified Correlation for Estimating Specific Chemical Exergy of Solid and Liquid Fuels. *Energy* **2012**, *40* (1), 164−173.
(35) Grønli, M. G.; Melaaen, M. C. Mathematical Model for Wood PyrolysisComparison of Experimental Measurements with Model Predictions. *Energy Fuels* **2000**, *14* (4), 791−800.
(36) https://www.engineeringtoolbox.com/specific-heat-solids-d_154.html (accessed Jan 19, 2024).
(37) Zhang, X.; Li, H.; Liu, L.; Bai, C.; Wang, S.; Zeng, J.; Liu, X.; Li, N.; Zhang, G. Thermodynamic and Economic Analysis of Biomass Partial Gasification Process. *Appl. Therm. Eng.* **2018**, *129*, 410−420.
(38) Eri, Q.; Wu, W.; Zhao, X. Numerical Investigation of the Air-Steam Biomass Gasification Process Based on Thermodynamic Equilibrium Model. *Energies* **2017**, *10* (12), 2163.
(39) Jayanarasimhan, A.; Pathak, R. M.; Shivapuji, A. M.; Rao, L. Tar Formation in Gasification Systems: A Holistic Review of Remediation Approaches and Removal Methods. *ACS Omega* **2024**, *9* (2), 2060−2079.
(40) Mountouris, A.; Voutsas, E.; Tassios, D. Solid Waste Plasma Gasification: Equilibrium Model Development and Exergy Analysis. *Energy Convers. Manage.* **2006**, *47* (13−14), 1723−1737.

https://doi.org/10.1021/acsomega.4c01687
ACS Omega 2024, 9, 32639−32650